

# Influence of boric acid concentration on the properties of electrodeposited CZTS absorber layers

M Y Zaki<sup>1,2,7</sup> , K Nouneh<sup>1</sup>, M Ebn Touhami<sup>2</sup>, E Matei<sup>3</sup>, P Badica<sup>4</sup> , M Burdusel<sup>4</sup>, C C Negrila<sup>5</sup>, M Baibarac<sup>6</sup>, L Pintilie<sup>3</sup> and A C Galca<sup>3,7</sup> 

<sup>1</sup>Laboratory of Physics of Condensed Matter, Faculty of Sciences, Ibn Tofail University, 14000 Kenitra, Morocco

<sup>2</sup>Laboratory of Materials and Environment Engineering: Modeling and Application, Faculty of Sciences, Ibn Tofail University, 14000 Kenitra, Morocco

<sup>3</sup>Laboratory of Multifunctional Materials and Structures, National Institute of Materials Physics, Atomistilor 405A, 077125 Magurele, Romania

<sup>4</sup>Laboratory of Magnetism and Superconductivity, National Institute of Materials Physics, Atomistilor 405A, 077125 Magurele, Romania

<sup>5</sup>Laboratory of Nanoscaled Condensed Matter, National Institute of Materials Physics, Atomistilor 405A, 077125 Magurele, Romania

<sup>6</sup>Laboratory of Optical Process in Nanostructured Materials, National Institute of Materials Physics, Atomistilor 405A, 077125 Magurele, Romania

E-mail: [mohamed.yassine.zaki@uit.ac.ma](mailto:mohamed.yassine.zaki@uit.ac.ma) and [ac\\_galca@infim.ro](mailto:ac_galca@infim.ro)

Received 9 August 2019, revised 20 December 2019

Accepted for publication 13 January 2020

Published 24 February 2020



## Abstract

This work involves the synthesis and characterization of  $\text{Cu}_2\text{ZnSnS}_4$  (CZTS) layers. The films were prepared on Mo/glass substrates by single-step electrodeposition method followed by sulfurization at 500 °C under argon flow. The effect of boric acid concentration on the crystallographic structure, compositional and morphological properties of CZTS films was investigated, with the objective to understand the growth behavior and to enhance the film properties. Cyclic Voltammetry was used in order to estimate the adequate deposition potential for the CZT alloy. The x-ray diffraction analysis showed the formation of the kesterite phase in all the samples. The Raman and x-ray photoelectron spectroscopy studies confirmed the existence of the CZTS phase. The scanning electron microscopy was employed to inspect the films structure. The results indicated that increasing the concentration of boric acid affects the physico-chemical properties of the films.

Keywords: CZTS, kesterite, electrodeposition

(Some figures may appear in colour only in the online journal)

## 1. Introduction

Copper zinc tin sulfide commonly known as CZTS, is a semiconductor material that is regarded as an excellent substitute for the current absorbers layers CIGS (copper indium gallium diselenide) and CdTe (cadmium telluride) for the next generation of p-type films of photovoltaic cells [1]. The rare

and toxic elements lead to economic and environmental issues to further develop CIGS and CdTe based solar cells. The CZTS films are composed of non-toxic and abundant cations, making this quaternary material a promising alternative and low cost absorber layer. Due to its suitable optical and electronic properties such as its direct band-gap (e.g. around 1.5 eV) [2, 3] and its high absorption coefficient, this chalcogenide material has been widely researched lately. Several techniques have been used to grow CZTS films, such as

<sup>7</sup> Authors to whom any correspondence should be addressed.

electrodeposition [4, 5], sputtering [6, 7], pulsed laser deposition [8], sol–gel [9], thermal evaporation [10], chemical bath deposition [11], spin coating [12], successive adsorption and reaction of ionic layers [13], or spray pyrolysis [14]. The world record efficiency of pure CZTS is (11%) so far [15], while a CZTSSe based photovoltaic cell was reported by IBM with (12.6%) efficiency [16]. These two values are still very far from the estimated theoretical conversion efficiency (32.2%) [1]. Electrodeposition of semiconductors has attracted a lot of attention since it offers a lot of advantages such as simplicity and low cost, and also scalability and manufacturability compared with vacuum-based processes. Among the electrodeposition parameters, the bath composition is the one which should be firstly explored and correlated with the properties of the deposited films. The role of the complexing agent in the electrochemical deposition is to facilitate the transfer toward the substrate surface and to improve the properties of the films [18, 19]. In this purpose, various works dealing with the effects of complexing agents have been done before, such as the comparison between different complexing agents [19, 23], the concentration of the used complexing agent [21, 22], and the combination between different complexing agents in the same electrolytic bath [24–26]. In a previous work the effect of combining trisodium citrate with several additives used as complexing agents was studied [27], and it was reported that the combination of trisodium citrate with both boric acid ( $\text{H}_3\text{BO}_3$ ) improves considerably the deposition of CZTS layers. Boric acid has been widely used in the electrodeposition of metals such as Cu, Zn and Sn and their alloys [28–30], while to our knowledge a use of different concentrations of boric acid in the electrodeposition of the CZT alloy was not yet reported. In this paper, we investigated the influence of multiple concentrations of boric acid. The structural, morphological and compositional characteristics of the prepared films were evaluated and discussed.

## 2. Experimental

In order to understand the reduction behaviors of the metals ions in the electrolyte and to define the optimal potential for the CZTS deposition, cyclic voltammetry (CV) was used in preliminary experiments. The electrochemical experiments were performed using a PGZ100 VoltaLab potentiostat and a three-electrode cell with a substrate of Mo/glass as working electrode, a platinum plate counter-electrode, and a saturated calomel electrode (SCE) as reference electrode as described in a previous work [27]. The electrolytic baths contained a solution of 0.03 M zinc sulfate heptahydrate ( $\text{ZnSO}_4 \cdot 7\text{H}_2\text{O}$ ), 0.02 M copper sulfate pentahydrate ( $\text{CuSO}_4 \cdot 5\text{H}_2\text{O}$ ), 0.02 M stannous chloride ( $\text{SnCl}_2$ ), 0.02 M sodium thiosulfate ( $\text{Na}_2\text{S}_2\text{O}_3$ ) and trisodium citrate ( $\text{Na}_3\text{C}_6\text{H}_5\text{O}_7$ ) as the main complexing agent in demineralized water. In addition to this different concentrations of boric acid ( $1 \times 10^{-2}$ ,  $2 \times 10^{-2}$  and  $5 \times 10^{-2}$  M) were added in order to find the right concentration that can offer consequently the best deposited CZTS films. The pH of the final solutions was adjusted to 5 by using citric acid. The solutions were magnetically stirred to

obtain a green, transparent and homogeneous mixture. The samples were deposited using a potentiostatic mode at room temperature by applying a potential of  $-1.15$  V with respect to the SCE electrode. The as deposited CZT samples were then inserted in a quartz tube along with elemental sulfur powder inside a tubular furnace. The thermal/sulfurization treatment was done in an argon atmosphere at  $500^\circ\text{C}$  for 1 h. The crystalline structure of CZTS films were inferred from the measurement done with a x-ray diffractometer (x-ray diffraction (XRD)) on a Bruker D8 Discover diffractometer in parallel beam setting, with monochromatic  $\text{Cu K}\alpha 1$  radiation ( $\lambda = 1.5406 \text{ \AA}$ ) and a Raman spectrometer, T64000 model, from Horiba Jobin Yvon equipped with a confocal Olympus BX41 microscope and an Ar laser (excitation wavelength of  $514 \text{ nm}$ ). The crystallite size was calculated from the (112) peak of XRD data using the Scherrer method, and the full width at half maximum (FWHM) was considered taking into account the instrumental broadening of the used instrument in the same configuration used to measure the CZTS samples, by measuring the standard NIST corundum sample, the FWHM of  $\alpha\text{-Al}_2\text{O}_3$  (012) reflection at  $2\theta = 25.58^\circ$  being  $\approx 0.157$ . Thus, the considered size contribution, FWHM was done by subtracting the instrumental value from the experimental one following the equation:  $\text{FWHM}_{(\text{size})} = \text{FWHM}_{(\text{exp})} - \text{FWHM}_{(\text{instru})}$ . Assuming an FWHM estimation error of  $0.02^\circ$ , the error of size determined by Scherrer approximation is around 2 nm. The surface morphology of the films was analyzed by scanning electron microscopy (SEM) using an EVO 50XVP system from Zeiss. XPS measurements were done using a monochromatic XR50M x-ray source operated at 300 W, 15 kV with a radiation energy of 1486.7 eV ( $\text{Al K}\alpha$ ) and a FWHM of 0.3 eV. The x-ray spot is smaller than the analyzed surface. The spectrometer is based on a PHOIBOS 150 hemispherical analyzer with an ultimate resolution of 0.44 eV (defined as FWHM of recorded  $\text{Ag } 3d_{5/2}$  spectral line). The spectra were calibrated using the C1s line ( $\text{BE} = 284.8 \text{ eV}$ ) of the absorbed hydrocarbon on the sample surface.

## 3. Results and discussion

First, the most favorable deposition potential of CZTS films at room temperature was estimated using CV. The CV was performed at an applied voltages range between  $-1.4$  and  $0.6$  V versus SCE with a scanning rate of  $50 \text{ mV s}^{-1}$  for different stirred electrolytic baths to understand the reactions between the complexing agents and the metal ions. The use of different concentrations of boric acid helps approximating the reduction potential of the CZT elements in the electrolyte and improves the deposition of metal alloys. Figure 1 shows cyclic voltammograms of the electrolyte without and with different concentrations of boric acid ( $0 \text{ M}$ ,  $1 \times 10^{-2} \text{ M}$ ,  $2 \times 10^{-2} \text{ M}$  and  $5 \times 10^{-2} \text{ M}$ ). From the CV measurements we can find that the reduction of  $\text{Cu}^{2+}$  ions is the same for all the electrolytes and starts approximately at  $-0.5$  V. Furthermore, the reduction of  $\text{Sn}^{2+}$  and  $\text{Zn}^{2+}$  ions is exactly the same without and with low concentration  $1 \times 10^{-2} \text{ M}$  of boric

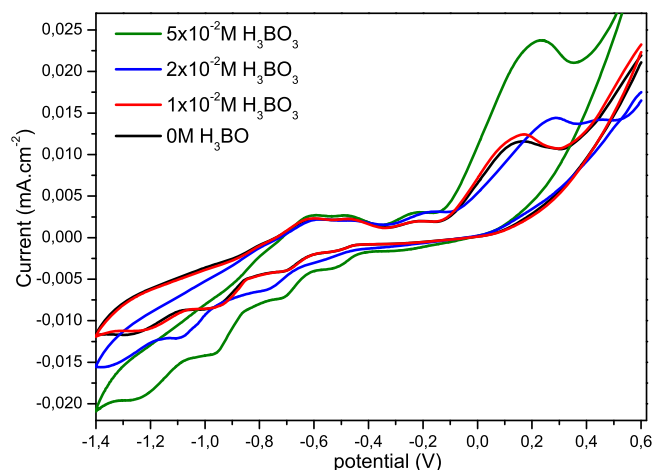


**Figure 1.** Cyclic voltammetry curves of CZT precursors at different concentration of  $\text{H}_3\text{BO}_3$ .

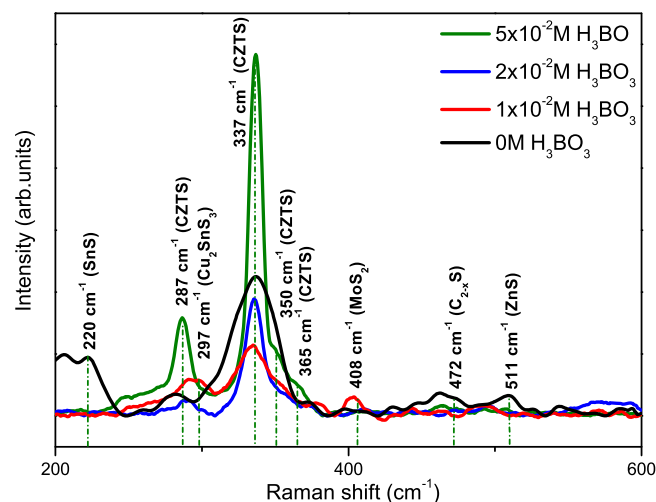


**Figure 3.** Raman spectra of CZTS films without and with various concentrations of  $\text{H}_3\text{BO}_3$ .

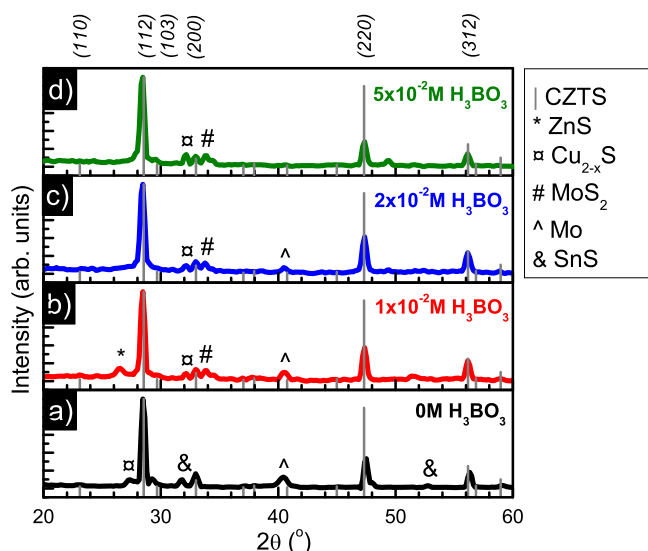


**Figure 2.** X-ray diffraction patterns of CZTS films without and with different concentrations of  $\text{H}_3\text{BO}_3$ .

**Table 1.** FWHM and crystallite size of the (112) plane of the CZTS samples obtained using different concentrations of boric acid.

Boric acid concentration	FWHM	Crystallite size (nm)
0 M	0.296	$27.7 \pm 2.0$ nm
$1 \times 10^{-2}$ M	0.291	$28.2 \pm 2.0$ nm
$2 \times 10^{-2}$ M	0.265	$30.9 \pm 2.0$ nm
$5 \times 10^{-2}$ M	0.231	$35.5 \pm 2.0$ nm

acid, and can be seen starting from  $-0.7$  V and  $-1$  V respectively. By adding a concentration of  $2 \times 10^{-2}$  M of  $\text{H}_3\text{BO}_3$  the reduction potential of the metal ions shifted to more negative values, especially for Sn and Zn deposition peaks that can be observed at  $-0.8$  V and  $-1.1$  V respectively. When the concentration of boric acid was increased to  $5 \times 10^{-2}$  M, the potential of deposition of  $\text{Sn}^{2+}$  and  $\text{Zn}^{2+}$  moved to less negative potentials and the peaks were observed at  $-0.6$  V and  $-0.95$  V respectively. It is worth

mentioning, that increasing the amount of boric acid leads to an increase in the current density, this might be due to the reduction of hydrogen caused by the adsorption of boric acid on the surface of the substrate, as boric acid can act as a catalyst and helps the electrodeposition of metal alloys [30]. Thus, the peak around  $-1.25$  V belongs to the hydrogen evolution. From figure 1 we can conclude that based on the CV the suitable deposition potential for the CZT elements, is around  $-0.5$  V for copper deposition, and  $-0.7$  to  $-0.8$  V for tin deposition, whereas the reduction potential of zinc is around  $-0.95$  to  $-1.1$  V. Therefore, since the reduction potential of zinc is lower comparing to copper and tin reduction potentials, the deposition potential of CZT films was fixed at  $-1.15$  V.

In order to explain the influence of boric acid concentration on the CZTS films, the samples were deposited with only trisodium citrate and with trisodium citrate mixed with boric acid as a second complexing agent ranging from  $1 \times 10^{-2}$  to  $5 \times 10^{-2}$  M. The XRD was used to identify the crystalline phases present in the films. Figures 2(a)–(d) shows XRD patterns of the CZTS films with only trisodium citrate and with different concentrations of boric acid. All samples contain the peaks (110), (112), (200), (220), and (312) that correspond to the kesterite structure CZTS according to (JCPDS 26-0575), as reported also in other previous studies [11, 32]. Since these peaks are the most prominent ones, it can be stated that all the samples are ‘close to pure’ CZTS films [33]. The Mo diffraction peak ( $2\theta = 40.5^\circ$ ) is also detected in all films. In figure 2(a) can be seen clearly the presence of the CZTS peaks mentioned before, while in addition, the presence of other peaks which can be attributed to the unwanted phases such as SnS ( $2\theta = 31.9^\circ$  and  $2\theta = 53.1^\circ$ ) (JCPDS 039-0354) and  $\text{Cu}_{2-x}\text{S}$  ( $2\theta = 27.8^\circ$ ) (JCPDS 23-0959). When boric acid was added in the solution, the same CZTS peaks are still present in figures 2(b)–(d) with the apparition of  $\text{MoS}_2$  ( $2\theta = 33.8^\circ$ ) due to the reaction of the Mo back contact with CZTS or sulfur [34, 35]. In addition a peak assigned to the secondary phase  $\text{Cu}_{2-x}\text{S}$  at ( $2\theta = 32.1^\circ$ ) is

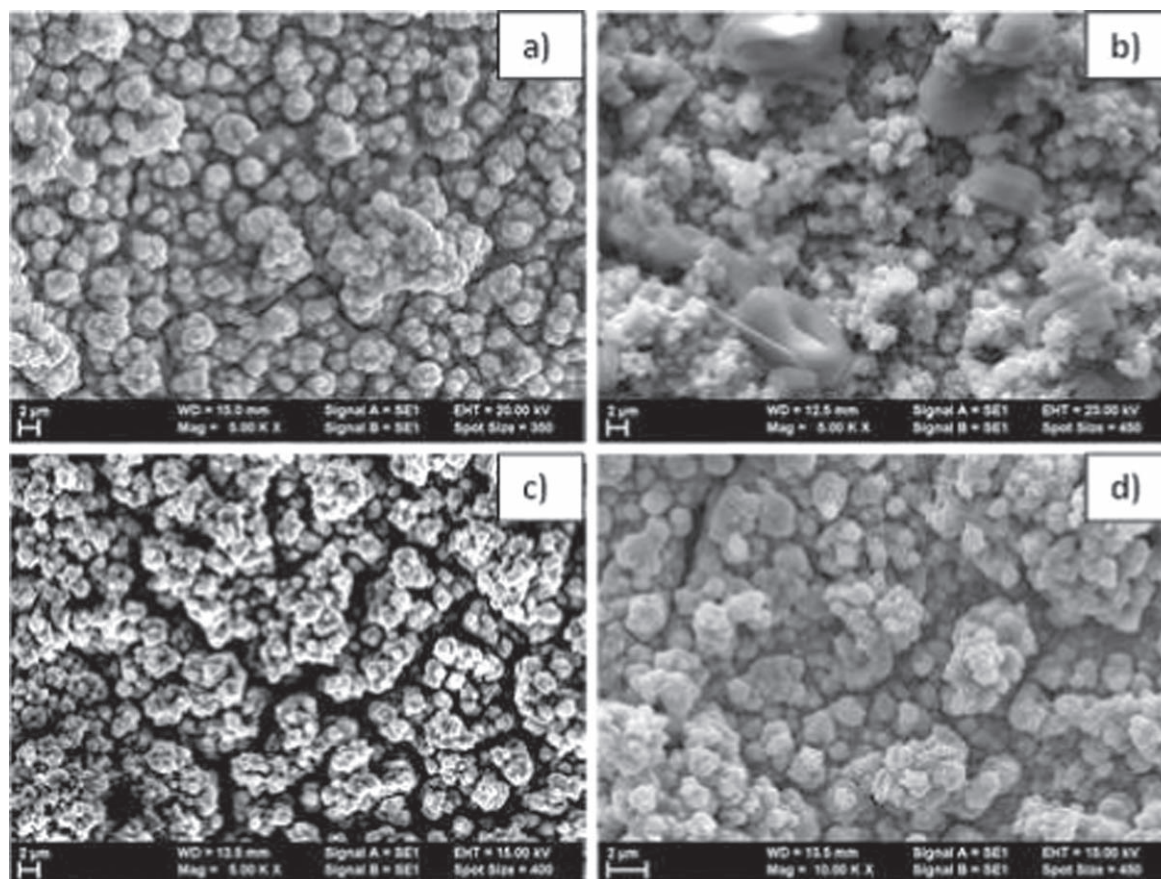


**Figure 4.** SEM micrographs of  $\text{Cu}_2\text{ZnSnS}_4$  films (a) without  $\text{H}_3\text{BO}_3$ , and with (b)  $1 \times 10^{-2} \text{ M}$   $\text{H}_3\text{BO}_3$ , (c)  $2 \times 10^{-2} \text{ M}$   $\text{H}_3\text{BO}_3$ , (d)  $5 \times 10^{-2} \text{ M}$   $\text{H}_3\text{BO}_3$ .

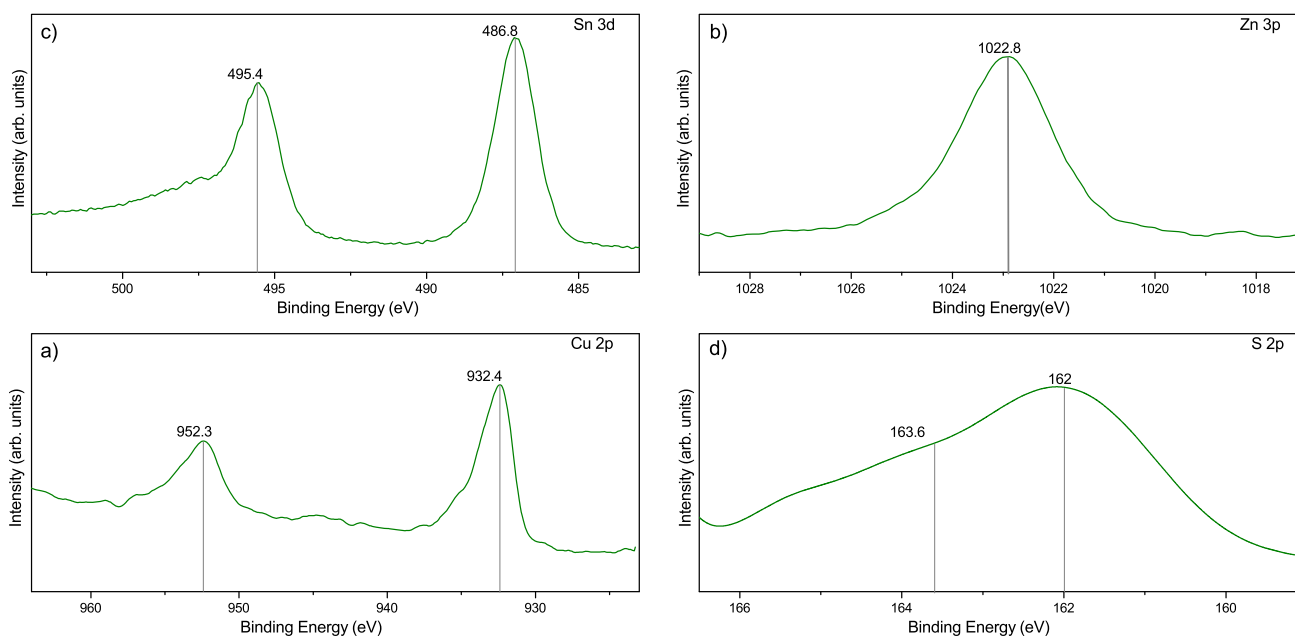


**Figure 5.** XPS spectra of the CZTS films deposited using  $5 \times 10^{-2} \text{ M}$   $\text{H}_3\text{BO}_3$ , (a) Cu 2p, (b) Zn 2p, (c) Sn 3d and (d) S 2p core levels.

observed in the three samples (JCPDS 23-0959). Also the sample with a  $1 \times 10^{-2}$  is the only one that might contain the cubic ZnS (the peak at  $2\theta = 26.9^\circ$ ) (JCPDS 036-1450). Several authors identified the presence of the same secondary

phases in CZTS samples [36, 37, 38], while in some studies solutions to get rid of those unwanted phases are proposed, as for copper sulfide being possible to remove it by immersing the samples in a KCN solution, the ZnS also can be removed



by using a solution of HCl [47], while for SnS, Xie *et al* [40] used a  $(\text{NH}_4)_2\text{S}$  solution. Figures 2(c) and (d) shows nearly the same pattern as the one from figure 2(b), however the ZnS peak is not detected in these two samples. Raising the concentration of boric acid to  $5 \times 10^{-2}$  M (figure 2(d)) leads to the emergence of a new tiny peak at  $2\theta = 29.6^\circ$  (JCPDS 26-0575) indicating that the sample is close to a single phase kesterite with an improved crystallinity. Therefore, to confirm the obtained XRD results, the size  $D$  of the crystallites was calculated from (112) peak of XRD data using the Scherrer formula:  $D = \frac{k\lambda}{\beta \cos(\theta)}$ , where  $D$  is the crystallite size,  $K$  is the Scherrer constant,  $\lambda$  is the wavelength of Cu  $K\alpha$  (0.154 06 nm),  $\beta$  is the corrected FWHM of the (112) peak and  $\theta$  is the Bragg angle. The results of the crystallite size calculations are presented in table 1. It was found that by rising the amount of boric acid, the FWHM values tend to decrease, leading to an increase of the crystallite size values. This improvement of particle size can be explained by the enhancement of the crystallinity of the samples [41] and this agrees with the XRD results. However, it is not easy to firmly confirm the pure kesterite phase existence since x-ray patterns of ZnS and CTS are overlapping the ones of CZTS [42]. In this view, Raman spectroscopy was performed to support the XRD results. Figure 3 shows the Raman spectra for CZTS films with only trisodium citrate and with combined trisodium citrate with multiple concentrations of boric acid. The existence of the kesterite phase is validated by the presence of the three Raman CZTS peaks situated around 287 and 337  $\text{cm}^{-1}$  [43, 44]. The peak around 408  $\text{cm}^{-1}$  is characteristic to the  $\text{MoS}_2$  phase [45, 47], evidencing that the sulfurization process affected also the Mo electrode. Without  $\text{H}_3\text{BO}_3$ , other peaks are present at 220  $\text{cm}^{-1}$  which can be attributed to SnS [48, 49] and at 472  $\text{cm}^{-1}$  that belongs to  $\text{Cu}_{2-x}\text{S}$  [50, 51]. By adding  $1 \times 10^{-2}$  M of  $\text{H}_3\text{BO}_3$ , additional peaks at 511  $\text{cm}^{-1}$  attributed to ZnS [52] and 297  $\text{cm}^{-1}$  attributed to  $\text{Cu}_2\text{SnS}_3$  [53] are visible, while the SnS peak is not present. The  $\text{Cu}_2\text{SnS}_3$  phase was undetectable by XRD as some minor phases cannot be inferred due to experimental limits [33, 48]. By increasing the amount of  $\text{H}_3\text{BO}_3$  to  $2 \times 10^{-2}$  M and  $5 \times 10^{-2}$  M the intensity of the main CZTS peak at 337  $\text{cm}^{-1}$  increases while the secondary phases peaks are less present, and the emergence of a small peak corresponding to the CZTS phase at 365  $\text{cm}^{-1}$  is observed. These changes in the Raman spectra signifies that the structure of the CZTS sample is characterized with a high crystalline quality [25, 55]. Increasing the amount of boric acid in the solution makes the CZTS films close to a pure kesterite phase with a good crystallinity and these results are in agreement with the above presented XRD results.

The morphology of the CZTS films was analyzed by using SEM. SEM images of CZTS films without and with different concentrations of boric acid onto Mo-coated glass substrates are presented in figures 4(a)–(d). The films prepared without boric acid (figure 4(a)) are formed of grains with different forms and sizes, while voids are also present. Figure 4(b) shows nearly the same morphology as the previous sample with a porous surface and different shaped and

sized grains. This inhomogeneity was also observed in previous works [56, 57] and might be due to the persistence of a variety of phases as reported also by Schorr *et al* [58]. By increasing the concentration of boric acid to  $2 \times 10^{-2}$  M (figure 4(c)), we can observe that the films consists of round shaped and larger grains with multiple voids and cracks. By adding more boric acid  $5 \times 10^{-2}$  M the sample surface (figure 4(d)) is quasi-homogeneous with less cracks and voids and larger grains compared with the previous cases. The presence of voids in all the samples might be caused by the reduction of hydrogen [59]. Thus, the boric acid concentration affects both the morphology and the grain size.

X-ray photoelectron spectroscopy (XPS) was employed to study the presence and the chemical state of the elements of the films surface. Figures 5(a)–(d) displays the binding energies of Cu 2p, Zn 2p, Sn 3d and S 2p of the CZTS sample respectively, with  $5 \times 10^{-2}$  M of boric acid. The two peaks at 932.4 eV and 952.3 eV which can be assigned to Cu  $2p_{3/2}$  and Cu  $2p_{1/2}$  respectively, shows the presence of Cu (I) [21]. The existence of Zn (II), can be confirmed by the core level Zn  $2p_{3/2}$  located at 1 022.8 eV [60]. Figure 5(c) shows the XPS spectra of the Sn3d, the peaks located at 486.8 eV and 495.4 eV refers to Sn  $3d_{5/2}$  and Sn  $3d_{3/2}$  respectively, and suggest the formation of Sn (IV) [61]. The binding energies of S (-II) consists of two peaks at 162 eV and 163.6 eV that corresponds to S  $2p_{3/2}$  and S  $2p_{1/2}$  respectively and confirms the presence of sulfur in the CZTS films [62]. One should note that the concentration of surface elements is different at the surface than in the bulk [63], due to the migration of some species (e.g. Zn) to the surface during the sulfurization process.




#### 4. Conclusion

CZTS films have been prepared by electrodeposition onto Mo/glass substrates in order to study the effect of boric acid used as complexing agents in the solution. The films were synthesized from electrodeposition bath containing different concentrations varied from  $1 \times 10^{-2}$  M to  $5 \times 10^{-2}$  M.  $\text{Cu}_2\text{SnS}_3$ ,  $\text{Cu}_{2-x}\text{S}$  and ZnS secondary phases are present in practically all samples along with  $\text{Cu}_2\text{ZnSnS}_4$  kesterite phase. ZnS being less representative of the existent secondary phases means that the samples are Zn poor and Cu/Sn rich. A nearly pure kesterite phase was obtained for the sample obtained by using  $5 \times 10^{-2}$  M of boric acid. Those results were inferred from XRD, and confirmed by XPS and Raman spectroscopy. Increasing the amount of boric acid has a significant effect on the surface morphology of the deposited films. The SEM images showed that the samples with an important amount of second complexing agent has a more homogeneous and compact surface but one should notice that cracks and cavities are still present in all the samples.

## Acknowledgments

MYZ acknowledges Romanian Ministry of Foreign Affairs and *Agence universitaire de la Francophonie* for the *Eugen Ionescu* research and mobility grant at NIMP. All authors acknowledge the Moroccan Ministry of Higher Education and Research and *Centre National pour la Recherche Scientifique et Technique* in the framework of PPR/37/2015 project, and the Romanian Ministry of Research and Innovation in the framework of Core Program PN19-03 (contract no. 21 N/08.02.2019) for the financial support.

## ORCID iDs

M Y Zaki  <https://orcid.org/0000-0002-8606-1140>  
 P Badica  <https://orcid.org/0000-0003-3038-2110>  
 A C Galca  <https://orcid.org/0000-0002-1914-4210>

## References

- [1] Suryawanshi M P, Agawane G L, Bhosale S M, Shin S W, Patil P S, Kim J H and Moholkar A V 2013 *Mater. Technol.* **28** 98–109
- [2] Malerba C et al 2014 *J. Alloys Compd.* **582** 528–34
- [3] Ferhati H and Djefall F 2018 *Opt. Mater.* **76** 393–9
- [4] Sugiarti S, Sjahriza A, Juniarti T and Firmansyah H 2018 *IOP Conf. Ser.: Earth Environ. Sci.* **187** 012082
- [5] Beres M, Syzdek J, Yu K M and Mao S S 2018 *Mater. Chem. Phys.* **204** 83–94
- [6] Balaji G, Balasundaraprabhu R, Prasanna S, Prabavathy N, McIlroy D N and Kannan M D 2018 *Opt. Mater.* **75** 56–60
- [7] Jiang J, Zhang L, Wang W, Huang X and Hong R 2018 *Mater. Sci. Semicond. Proc.* **83** 125–32
- [8] Cazzaniga A C et al 2017 *Sol. Energy Mater. Sol. C* **166** 91–9
- [9] Agawane G L, Kamble S A, Vanalakar S A, Shin S W, Gang M G, Yun J H, Gwak J, Moholkar A V and Kim J H 2015 *Mater. Lett.* **158** 58–61
- [10] Wang K, Gunawan O, Todorov T, Shin B, Chey S J et al 2010 *Appl. Phys. Lett.* **97** 143508
- [11] Henry J, Mohanraj K and Sivakumar G 2017 *Optik* **141** 139–45
- [12] Gadallah A S, Salim M A, Atwee T and Ghander A M 2018 *Optik* **159** 275–82
- [13] Henry J, Mohanraj K and Sivakumar G 2016 *J. Asian Ceram. Soc.* **4** 81–4
- [14] Diwate K, Mohite K, Shinde M, Rondiya S, Pawbake A, Date A, Pathan H and Jadkar S 2017 *Energy Proc.* **110** 180–7
- [15] Yan C et al 2018 *Nat. Energy* **3** 764–72
- [16] Wang W, Winkler M T, Gunawan O, Gokmen T, Todorov T K, Zhu Y and Mitzi D B 2013 *Adv. Energy Mater.* **4** 1301465
- [17] Rodriguez C A, Tobosque P, Maril M, Camurri C, Basaez L, Delplanck M P and Carrasco C 2017 *J. Mater. Sci.* **52** 3388–401
- [18] Mkawi E M, Ibrahim K, Ali M K M, Farrukh M A, Mohamed A S and Allam N K 2014 *J. Electroanal. Chem.* **735** 129–35
- [19] Azmi S, Nohair M, El Marrakchi M, Khoumri E M and Dabala M 2018 Effect of the complexing agents on the properties of electrodeposited czts thin films *7th Int. Conf. on Renewable Energy Research and Applications* pp 1346–51
- [20] Pawar B S, Pawar S M, Shin S W, Choi D S, Park C J, Kolekar S S and Kim J H 2010 *Appl. Surf. Sci.* **257** 1786–91
- [21] Chaudhari J J and Joshi U S 2018 *Appl. Phys. A* **124** 465
- [22] Toura H, Khattak Y H, Baig F, Soucase B M, Ebn Touhami M and Hartiti B 2019 *Curr. Appl. Phys.* **19** 606–13
- [23] Tao J, Chen L, Cao H, Zhang C, Liu J, Zhang Y, Huang L, Jiang J, Yang P and Chu J 2016 *J. Mater. Chem. A* **4** 3798–805
- [24] Guo Y, Wei J, Liu Y, Yang T and Xu Z 2017 *Nanoscale Res. Lett.* **12** 181
- [25] Zaki M Y, Nouneh K, Ebn Touhami M, Belakhmima R A, Galca A C, Pintilie L, Enculescu M, Baibarac M and Taibi M 2018 *Opt. Mater.* **83** 252–6
- [26] Heidari G, Khoie S M M, Abrishami M E and Javanbakht M 2015 *J. Mater. Sci.: Mater. Electron.* **26** 1969–76
- [27] Pushpavanam M and Balakrishnan K 1996 *J. Appl. Electrochem.* **26** 283–90
- [28] Zheng-zhong Z, Xiao-rong Z and Chao Z 1999 *Wuhan Univ. J. Nat. Sci.* **4** 211–5
- [29] Buldu D G, Cantas A, Turkoglu F, Akca F G, Meric E, Ozdemir M, Tarhan E, Ozyuzer L and Aygun G 2018 *Phys. Scr.* **93** 024002
- [30] Berg D M, Arasimowicz M, Djemour R, Gutay L, Siebentritt S, Schorr S, Fontane X, Izquierdo-Roca V, Perez-Rodriguez A and Dale P J 2014 *Thin Solid Films* **569** 113–23
- [31] Cui H, Lee C Y, Li W, Liu X, Wen X and Hao X 2015 *Int. J. Photoenergy* **2015** 1–9
- [32] Yang K J, Sim J H, Son D H, Kim D H, Kim G Y, Jo W, Song S, Kim J H, Nam D, Cheong H and Kang J K 2015 *Prog. Photovolt.* **23** 1771–84
- [33] Irkhina A, Levchenko S, Hinrichs V, Plate P and Unold T 2017 *RSC Adv.* **7** 11752–60
- [34] Bhosale S M, Suryawanshi M P, Kim J H and Moholkar A V 2015 *Ceram. Int.* **41** 8299–304
- [35] Muska K, Kauk M, Altosaar M, Pilvet M, Grossberg M and Volobujeva O 2011 *Energy Proc.* **10** 203–7
- [36] Fairbrother A, Izquierdo-Roca V, Fontané X, Ibáñez M, Cabot A, Saucedo E and Pérez-Rodríguez A 2014 *Cryst. Eng. Comm.* **16** 4120–5
- [37] Xie H, Sanchez Y, Lopez-Marino S, Espindola-Rodriguez M, Neuschitzer M, Sylla D, Fairbrother A, Izquierdo-Roca V, Perez-Rodriguez A and Saucedo E 2014 *ACS Appl. Mater. Interfaces* **6** 12744–51
- [38] Ren Y, Scragg J J, Frisk C, Larsen J K, Li S Y and Platzer-Bjorkman C 2015 *Phys. Status Solidi a* **212** 2889–96
- [39] Covei M, Perniu D, Bogatu C and Duta A 2019 *Catal. Today* **321–322** 172–7
- [40] Chen S, Tao J, Tao H, Shen Y, Zhu L, Jiang J, Zeng X and Wang T 2015 *Mater. Technol.* **30** 306–12
- [41] Singh O P, Muhunthan N, Singh V N, Samanta K and Dilawar N 2014 *Mater. Chem. Phys.* **146** 452–5
- [42] Li H, Zhang Q, Yap C C R, Tay B K, Edwin T H T, Olivier A and Baillargeat D 2012 *Adv. Funct. Mater.* **22** 1385–90
- [43] Mahajan S, Stathatos E, Huse N, Birajdar R, Kalarakis A and Sharma R 2018 *Mater. Lett.* **210** 92–6
- [44] Su C Y, Chiu C Y and Ting J M 2015 *Sci. Rep.* **5** 9291
- [45] Fernandes P A, Salome P M P and da Cunha A F 2011 *J. Alloys Compd.* **509** 7600–6
- [46] Zutz F, Chory C, Knipper M, Parisi J, Riedel I, Izquierdo-Roca V, Fontané X and Pérez-Rodríguez A 2014 *Phys. Status Solidi a* **212** 329–335
- [47] Nishida G, Murayama M, Takeuchi A, Shimamune Y, Jimbo K and Katagiri H 2018 *Japan. J. Appl. Phys.* **57** 08RC03

- [52] Nilsen W G 1969 *Phys. Rev.* **182** 838–50
- [53] Berg D M, Djemour R, Gutay L, Siebentritt S, Dale P J, Fontane X, Izquierdo-Roca V and Perez-Rodriguez A 2012 *Appl. Phys. Lett.* **100** 192103
- [54] Wadhene R, Assaker I B and Chtourou R 2018 *J. Mater. Sci. Mater. Electron.* **29** 17374–87
- [55] Yao L *et al* 2019 *Crystals* **9** 10
- [56] Olgar M A, Klaer J, Mainz R, Ozyuzer L and Unold T 2017 *Thin Solid Films* **628** 1–6
- [57] Engberg S, Canulescu S and Schou J 2018 *RSC Adv.* **8** 7152–8
- [58] Schorr S, Gurieva G, Guc M, Dimitrievska M, Perez-Rodriguez A, Izquierdo-Roca V, Schnohr C S, Kim J, Jo W and Merino J M 2019 *J. Phys.: Energy* **2** 012002
- [59] Tsai W L, Hsu P C, Hwu Y, Chen C H, Chang L W, Je J H, Lin H M, Groso A and Margaritondo G 2002 *Nature* **417** 139
- [60] Zhang X, Shi X, Ye W, Ma C and Wang C 2009 *Appl. Phys. A* **94** 381
- [61] Xu J, Yang X, Yang Q D, Wong T L and Lee C S 2012 *J. Phys. Chem. C* **116** 19718–23
- [62] Dai P, Shen X, Lin Z, Feng Z, Xu H and Zhan J 2010 *Chem. Commun.* **46** 5749–51
- [63] Cantas A, Turkoglu F, Meric E, Akca F G, Ozedmir M, Tarhan E, Ozyuzer L and Aygun G 2018 *J. Phys. D: Appl. Phys.* **51** 275501